QCS2019 Sep. 25-28. Busan Korea

中国科学院新疆天文台
XINJIANG ASTRONOMICAL OBSERVATORY, CAS

The surface thermal emission and crust magnetic field decay in magnetars

Zhifu Gao and Na Wang

Xinjiang Astronomical Observatory, Chinese Academy of Sciences, Urumqi, Xinjiang, China

ications of the Astronomical Society of the Pacific, 131:054201 (17pp), 2019 May https://doi.org/10.1088/1538-3873/ab0440
9. The Astronomical Society of the Pacific. All rights reserved. Printed in the U.S.A.

Investigations of the Ohmic Decay and the Soft X-Ray Emission of the High-braking-index Pulsar PSR J1640−4631

Hui Wang[1,2], Zhifu Gao[3], Na Wang[3], Huanyu Jia[1], Xiangdong Li[4], and Qijun Zhi[2,5]
[1] School of Physical Science and Technology, Southwest Jiaotong University, Chengdu 610031, People's Republic of China; hyjia@swjtu.cn
Guizhou Provincial Key Laboratory of Radio Astronomy and Data Processing, Guizhou Normal University, Guiyang 550001, People's Republic of China
[3] Xinjiang Astronomical Observatory, Chinese Academy of Sciences, 150, Science 1-Street, Urumqi, Xinjiang 830011, People's Republic of China
zhifugao@xao.ac.cn
Department of Astronomy and Key Laboratory of Modern Astronomy and Astrophysics, Nanjing University, Jiangsu 210046, People's Republic of China
[5] School of Physics and Electronic Science, Guizhou Normal University, Guiyang 550001, People's Republic of China
Received 2018 March 17; accepted 2019 February 4; published 2019 March 20

Abstract

The young pulsar PSR J1640−4631 is the first pulsar reported with a high braking index, $n = 3.15 \pm 0.03$, and has attracted extensive attention. In this work, by inputting the equation of state, we obtain two typical and feasible ranges of the electrical conductivity in the crust of PSR J1640−4631. Then, by considering the effects of general relativity, we formulate the induction equation and use it to investigate the decay of crustal magnetic fields within two scenarios: pure Ohmic decay, and the combination of Ohmic decay and Hall drift. In the former scenario, we calculate the current magnetic field decay rates as $dB_p/dt \sim (0.78–1.00) \times 10^7$ G yr^{-1} and $dB_t/dt \sim (0.82–1.05) \times 10^8$ G yr^{-1} for the poloidal and toroidal parts, respectively, and estimate the current magnetic energy decay rate as $L_B \sim (0.95–1.22) \times 10^{32}$ erg s^{-1}. In the latter scenario, the combination of Ohmic decay and Hall drift accelerates the decay of magnetic fields, and we calculate the current magnetic field decay rates as $dB_p/dt \sim (1.26–1.47) \times 10^7$ G yr^{-1}, and $dB_t/dt \sim (1.32–1.54) \times 10^8$ G yr^{-1} for the poloidal and toroidal parts, respectively, and estimate the current magnetic energy decay rate as $L_B \sim (1.86–2.18) \times 10^{32}$ erg s^{-1}. It is found that the recalculated value of the braking index n of the star is lower than its observed value, which implies that other factors influence the spin-down evolution. The current magnetic energy decay rates calculated in both scenarios are far less than the isotropic soft X-ray luminosity obtained from *Chandra*+*NuStar* telescopes. The observed soft X-ray flux in the (2–10) keV band is $F_X \sim 1.8(4) \times 10^{-13}$ erg cm^{-2} s^{-1}, which corresponds to a high surface temperature, $T \sim 1.54(6) \times 10^6$ K. The observed X-ray flux of the star could be caused by the decay of a multipolar magnetic field near the pole, which is strong enough to activate the slot-gap mechanism. The high surface temperature of the star is attributed either to magnetic spot formation or thermoplastic wave heating due to the decay of the toroidal field near the pole. Our results

Electrical conductivity of the magnetar crust

- The electrical conductivity, σ, in the crust of a neutron star (NS) is defined by

$$\frac{1}{\sigma}=\frac{1}{\sigma_{hp}}+\frac{1}{\sigma_{imp}}, \qquad (1)$$

where σ_{hp} and σ_{imp} are conductivities due to the electron-phonon scattering and electron-impurity scattering, respectively.

- The crustal conductivity depends strongly on the temperature, T, and the density, ρ, which spans six orders of magnitude or above. A third parameter for determining σ is the impurity concentration, Q.

- In this work we implement realistic conductivity profiles provided by Potekhin \& Chabrier (2013) into the code to produce more reliable magnetic field decay results. Here we choose the BBP model (Baym, Bethe \& Pethick 1971) to be the equation of state (EoS) of the magnetar's inner crust.

Fig1. Crustal conductivity in ultrastrong magnetic fields

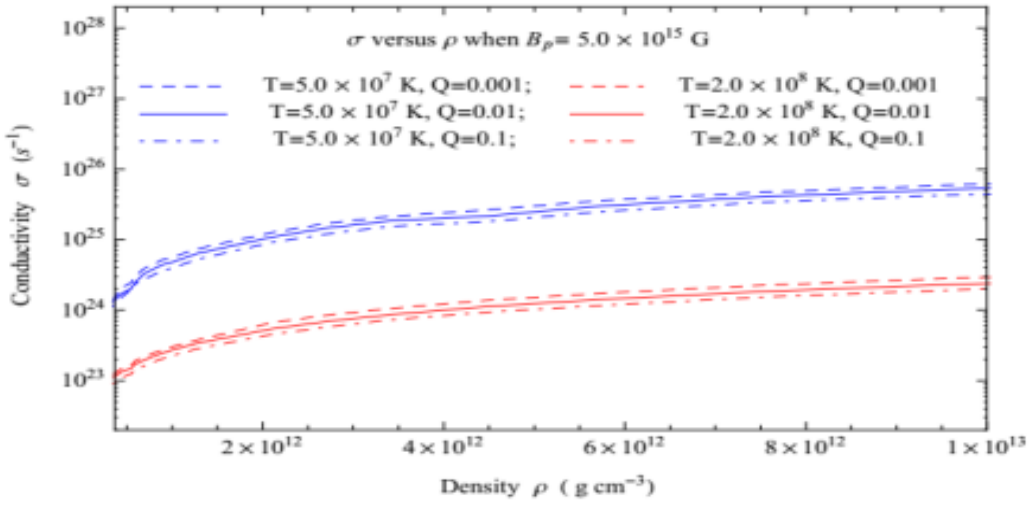

(a)

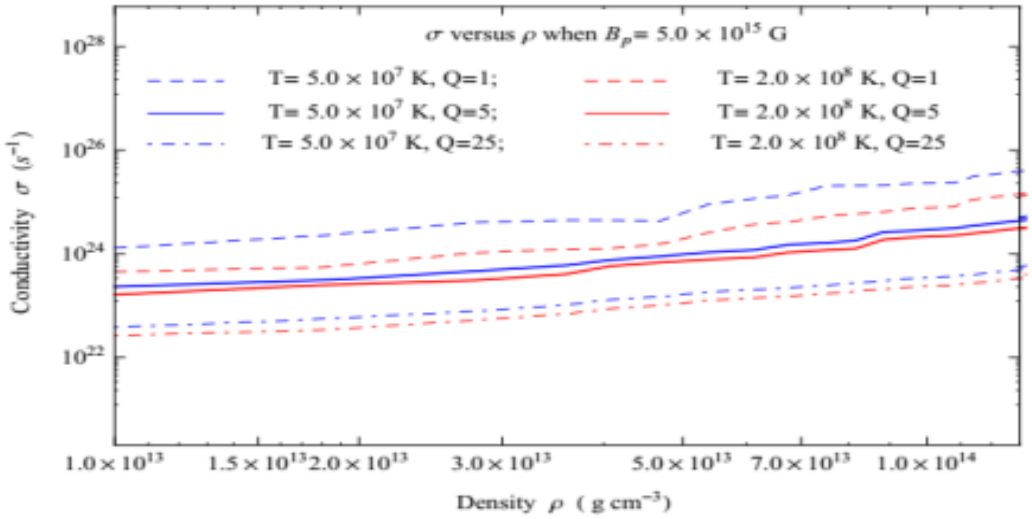

(b)

Our methods

Here we use the BBP and TMA EOSs, and choose a magnetar with a typical mass of $M=1.45M_{\odot}$, corresponding to $R=11.77\,\mathrm{km}$, $R_{crust}\sim 0.98\,\mathrm{km}$ and $\mu=1.676$. From Eq.(15) and Eq.（33）of WGW19， we get the decay rates of toroidal magnetic field and poloidal magnetic field,

$$\frac{dH}{dt}=\frac{-\mu x c^2\lambda_n}{8\pi\sigma R}\sum_n A_n\frac{j_1(n\pi x)}{x^2R^2}e^{\frac{-c^2\lambda_n t}{4\pi\sigma R^2}},\quad \frac{dB}{dt}=\frac{-c^2\lambda_n}{4\pi\sigma R}\sum_n A_n\frac{j_1(n\pi x)}{x^2R^2}e^{\frac{-c^2\lambda_n t}{4\pi\sigma R^2}}\quad 。\qquad (2)$$

where A_n is the expansion coefficient $A_n=\int_0^1 x j_1(n\pi x)x^2dx/(\int_0^1 j_1^2(n\pi x)x^2dx)$, $j_1(\zeta)=\frac{1}{\zeta^2}(\sin\zeta-\xi\cos\xi)$ is the first order spherical Bessel function, λ_n is determined by the associated boundary-regularity conditions. The magnetic energy decay rates, which are also functions of *t*, can now be estimated from

$$L_{p/t}=\frac{-1}{4\pi}\int_V B_{p/t}\frac{dB_{p/t}}{dt}dV\ , \qquad (3)$$

where $dV=4\pi r^2dr$, $R_{crust}\sim 0.98\,\mathrm{km}$. **Inserting** $\sigma=2.52\times10^{-24}\ \mathrm{s}^{-1}$ **and** $\sigma=8.75\times10^{24}\ \mathrm{s}^{-1}$ **into Eqs (2) and (3) , using numerically simulating, we get the diagrams of** B_p-t、B_p-t、dB_p/dt、dB_t/dt、L_p-t **and** L_t-t **in two cases of** $B_p(0)=3.0\times10^{15}$ G **and** $B_p(0)=5.0\times10^{14}$ G **.**

Our results

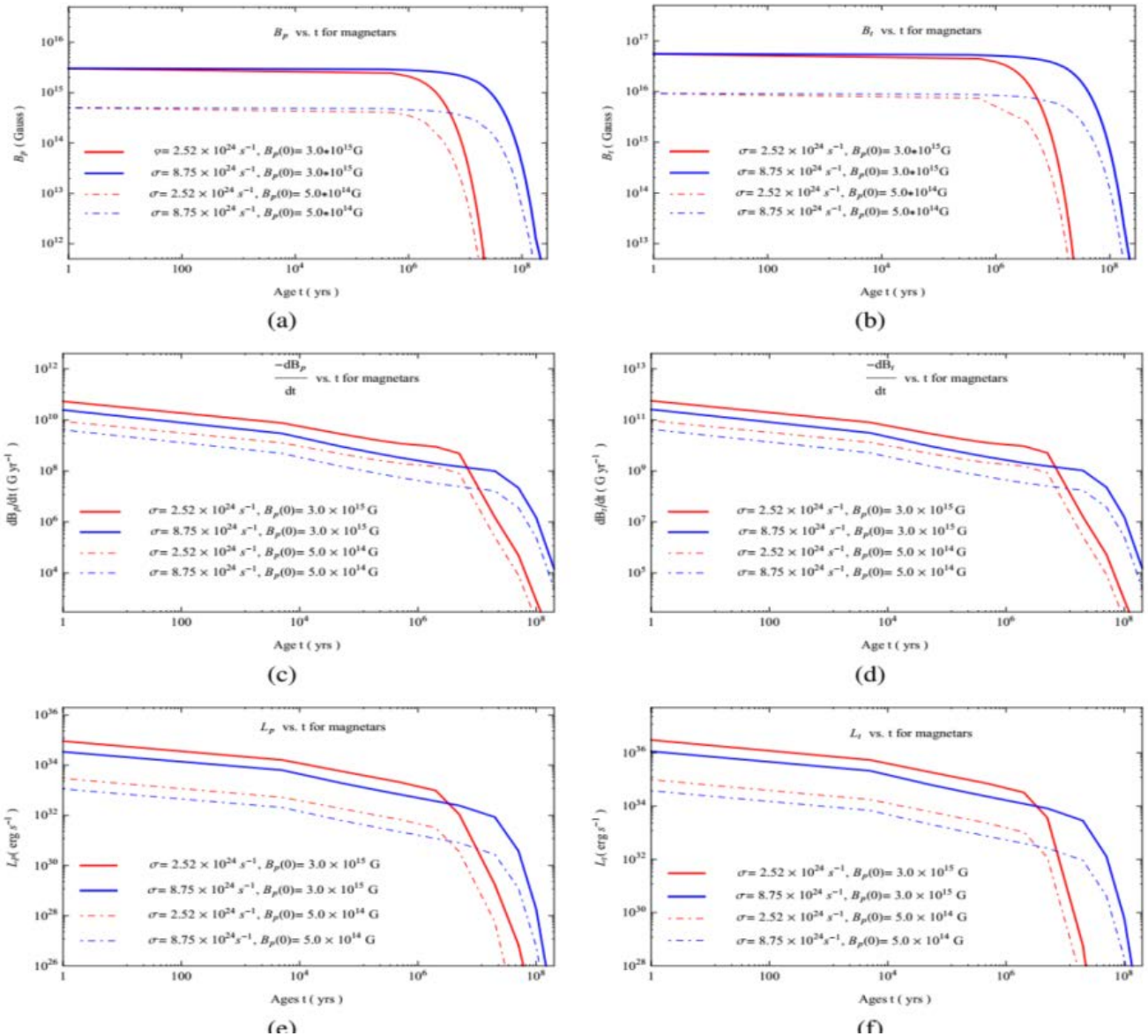

Figure 3. Numerical fitting of Ohmic decay formagnetars. (a) The poloidal magnetic field, B_p, as a function of t *at* x=1; (b) the toroidal magnetic field, B_t, as a function of t at x1; (c) the poloidal magnetic field decay rate, dB_p/dt , as a function of t at x=1; (d) the toroidal magnetic field decay rate, dB_t/dt, as a function at x=1; (e) the poloidal magnetic filed energy decay rate, L_p, as a function of t, and (e) the toroidal magnetic filed energy decay rate, L_t, as a function of t. The red and blue solid lines in (b)–(d) indicate $\sigma = 2.52 \times 10^{24}\,\mathrm{s}^{-1}$ and $\sigma = 8.75 \times 10^{24}\,\mathrm{s}^{-1}$, respectively

Compared with observations

TABLE 1 The persistent timing, ages and emission characteristics for 22 magnetars candidates with observed soft X-ray flux. All data are referred to http://www.physics.mcgill.ca/~ pulsar/magnetar/main.html.

Source	P (s)	$\dot{P}$ (10^{-11} s/s)	τ_c (kyr)	Age Eest. (kyr)	Assoc.	Method	L_X (erg s^{-1})	L_{rot} (erg s^{-1})
1E 2259+586	6.97904	0.04837	230.0	10–20	CTB 109	SNR	1.70×10^{34}	7.37×10^{31}
4U 0142+61	8.68870	0.2022(4)	68.00	68	SMC	τ_c	1.05×10^{35}	1.85×10^{32}
CXOU J164710	10.61	< 0.04	> 420.0	420	MC 13A	τ_c	4.50×10^{32}	4.65×10^{31}
1E1048.1–5937	6.45787	2.250	4.50	4.50	GSH 2883.3-0.5-28	τ_c	4.90×10^{34}	4.65×10^{33}
CXOU J010043	8.0204	1.88(8)	6.800	6.8	SMC	τ_c	6.50×10^{34}	2.33×10^{33}
1RXSJ170849	11.005	1.9455(13)	9.000	9.0	Westerlund1	τ_c	4.20×10^{34}	7.37×10^{32}
1E1841–045	11.7889	4.092(15)	4.700	0.50–1.00	Kes 73	SNR	1.84×10^{35}	1.47×10^{33}
SGR 0501+4516	5.76206	0.594(2)	16.0	4–6	HB9	SNR	8.10×10^{32}	1.85×10^{33}
SGR 0526–66	8.0544(2)	3.8(1)	3.400	4.8	N49	SNR	1.89×10^{35}	4.22×10^{33}
SGR 1900+14	5.19987	9.2(4)	0.900	3.98–7.94	Cluster	Pro.Mot.	9.00×10^{34}	3.79×10^{34}
SGR 1806–20	7.54773	49.5000	0.240	0.63–1.0	W31	Pro.Mot.	1.63×10^{35}	6.68×10^{34}
SGR 0418–5729	9.07839	0.0004(1)	36000	550	SNR	τ_c	9.60×10^{29}	3.10×10^{29}
XTE J1810–197	5.54035	0.777(3)	11	11	W31	τ_c	4.3×10^{31}	2.93×10^{35}
1E 1547.0–5408	2.07212	4.77	0.69	0.63	G327.24–013	SNR	1.3×10^{33}	3.11×10^{35}
CXOU J171405	2.07212	4.77	0.95	5	CTB 37B	SNR	5.6×10^{34}	6.13×10^{34}
SGR 1627–41	2.59458	1.9(4)	2.2	5.0	G337.0–0.1	SNR	3.6×10^{33}	5.87×10^{34}
3XXM J185246	11.587	< 0.014	> 1300	5 – 7	Kes79	SNR	$< 4.0\times10^{32}$	$< 3.6\times10^{30}$
Swift J1822	8.43772	0.0021(2)	6300	6300	HII region	τ_c	$< 4.0\times10^{29}$	2.0×10^{30}
Swift J1834	2.4823	0.796(12)	4.9	60–200	W41	SNR	$< 8.4\times10^{30}$	3.1×10^{34}
PSR J1622–4950	4.326(1)	1.7(1)	4.0	≤ 6.0	G333.9+0.0	SNR	4.40×10^{34}	1.18×10^{34}
SGR J1745–2900	3.7636	1.385(15)	4.30	4.30	Galaxy Center	τ_c	1.10×10^{32}	1.47×10^{34}
PSR J1846–0258	0.32657	0.71070	0.73	0.9	Kes75	SNR	1.90×10^{34}	8.10×10^{36}

From the McGill Online Magnetar Catalog on April 2019, (http://www.physics.mcgill.ca/~pulsar/magnetar/main.html), one can see that there are 21 magnetars and magnetar candidates with persistent X-ray phonons, as listed in Table 2. The soft X-ray luminosity L_X^{∞} is estimated by $L_X^{\infty}=4\pi D^2 (F_X^{\infty})^4$, where D is the source distance and F_X^{∞} is the unabsorbed X-ray flux in the 0.5-10 keV range. The rotational energy loss rate is defined as $L_{rot}=I\Omega\dot{\Omega}=4\pi^2 I\nu\dot{\nu}=-4\pi^2 I \dot{P} P^{-3}$, where the moment of inertial is taken as $I=1.47(2)\times 10^{45}$ g cm^2 assuming a medium-mass NS with $M=1.45M_{\odot}$ in the TMA model, Ω is the angular velocity, and $\dot{\Omega}$ is the derivative of Ω,$\nu=\Omega/2\pi$ is the spin-frequency and P is the spin-period.

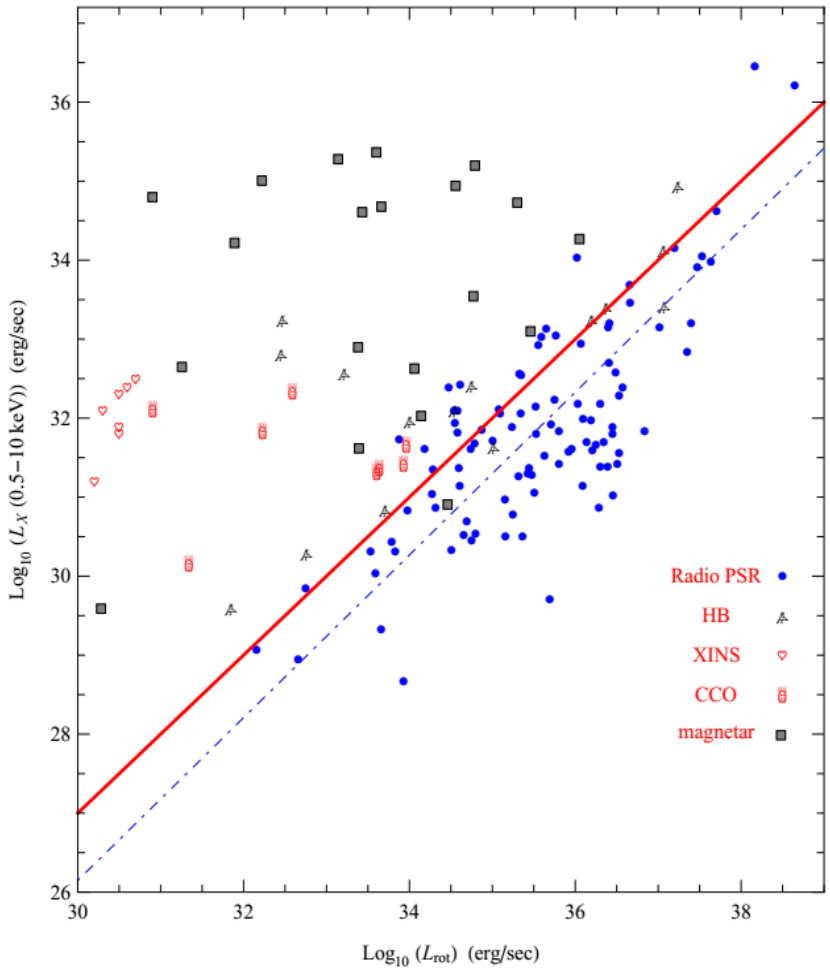
Log10 (LX (0.5−10 keV)) (erg/sec)
Log10 (Lrot) (erg/sec)
Radio PSR
HB
XINS
CCO
magnetar

(a)

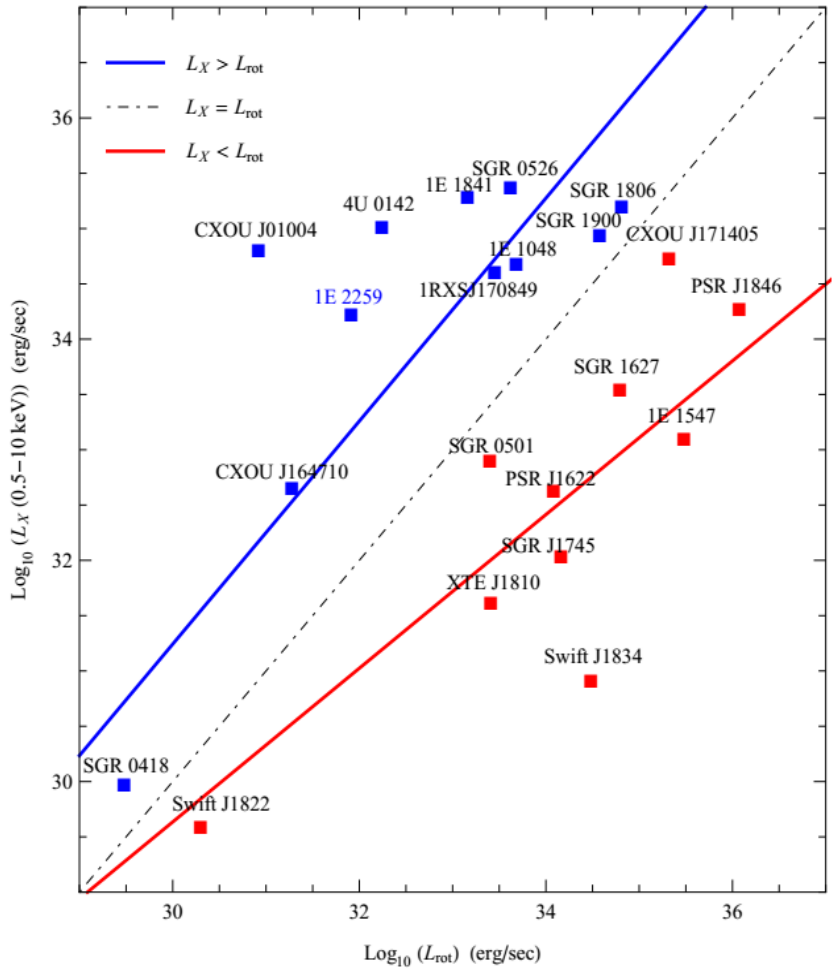
LX > Lrot
LX = Lrot
LX < Lrot
SGR 0526
1E 1841
SGR 1806
4U 0142
SGR 1900
CXOU J01004
CXOU J171405
1E 1048
1E 2259
1RXS J170849
PSR J1846
SGR 1627
1E 1547
SGR 0501
CXOU J164710
PSR J1622
SGR J1745
XTE J1810
Swift J1834
SGR 0418
Swift J1822
Log10 (LX (0.5−10 keV)) (erg/sec)
Log10 (Lrot) (erg/sec)

(b)

The X-ray conversion coefficient is estimated as

$$\eta = F_X^s/(L_B) = F_X^\infty/((1 - r_g/R)L_B),$$

where F_X^S is the surface X-ray luminosity without redshift and $r_g = GM/c^2$ is the Schwarzschild radius. Assuming an isotropic X-ray emission and taking $R = R_{NS}$, we can estimate the magnetar surface temperatures in theory via $T_s^\infty = T_s(1 - r_g/R)^{1/2}$ and $\eta L_B = 4\pi R^2 \sigma_s T_s^4$ with σ_s the Stefan-Boltzmann constant. Using Eq.(10), we obtain the range of magnetic field energy release, $L_B = L_t + L_p \sim L_t = (2.26 \times 10^{32} - 3.84(6) \times 10^{36})\,\mathrm{erg\,s^{-1}}$, the X-ray conversion coefficient $\eta \sim 10^{-2} - 10^{-1}$ for 11 magnetars. Then we get the range of magnetar surface temperatures,$T_s^\infty = (\eta/0.2)^{\frac{1}{4}} \times (2.7 - 6.8) \times 10^6$ K=$(\eta/0.2)^{\frac{1}{4}} \times (0.23 - 0.61)$ keV, which approaches to the range of observed magnetars'surface temperatures (see in Table 2).

TABLE 2

Source	D kpc	F_X^{∞} erg s^{-1}cm^{-2}	T_{BB} keV	$B_p(0)$ 10^{14}G	Age Est. kyr	Method	L_B^a erg s^{-1}	η^a %	L_B^b erg s^{-1}	η^b %
SGR0418–5729	2.00	2.00×10^{-11}	0.30	3.00	550	modeling	2.26E32	0.31	5.35E32	0.74
1E 2259+586	3.2(2)	1.41×10^{-11}	0.37(1)	5.00	15(5)	SNR	1.4(3)E35	22(6)	6.5(1.0)E35	47(8)
4U 0142+614	3.6(4)	6.97×10^{-11}	0.41	30.0	68.0	τ_c	1.14E36	15	4.85E35	37
CXOU J164710	3.9(7)	2.54×10^{-11}	0.59(6)	3.00	158.0	pro.mot	8.65E33	9	3.62E33	21
1E 1048–5937	9.0(1.7)	5.11×10^{-11}	0.56(1)	10.0	4.50	τ_c	7.19E35	12	3.08E35	27
CXOU J010043	62.4(1.6)	1.40×10^{-11}	0.30(2)	10.0	6.80	τ_c	6.82E35	16	3.22E35	34
3XXM J185246	7.1	1.0×10^{-11}	0.6	3.0	6(1)	SNR	3.53E33	11.3	2.11E33	18.8
1RXS J170849	3.8(5)	2.43×10^{-11}	0.456	10.0	9.00	τ_c	7.65E35	9	3.23E35	21
1E1841–045	8.6(1.1)	2.13×10^{-11}	0.45(3)	10.0	0.75(2.5)	SNR	1.2(2)E36	26(4)	5.9(7)35	46(4)
SGR 0526–66	53.6(1.2)	5.50×10^{-11}	0.44(2)	30.0	4.80	SNR	2.28E36	8	7.11E35	26
SGR 1900+14	13.0(1.2)	4.82×10^{-12}	0.47(2)	30.0	6(2)	pro.mot	2.2(6)E36	7(1)	7.8(8)E35	19(2)
SGR 1806–20	8.8(1.6)	1.81×10^{-12}	0.55(7)	30.0	0.8(2)	pro.mot.	3.8(4)E36	7.4(8)	8.9(9)E35	26(2)

Footnote:[a] This denotes the case of $\sigma = 2.25 \times 10^{24}\,\mathrm{s}^{-1}$ Footnote:[b] This denotes the case of $\sigma = 8.75 \times 10^{24}\,\mathrm{s}^{-1}$.[c] SGR 0418+5729 is the lowest magnetic field magnetar with the dipole field at the equator $B_d \simeq 6 \times 10^{12}$ G (Rea et al. 2013). The X-ray flux of this source has decreased by about four orders of magnitude (from about 1.4×10^{-11} to $(1 - 3.4) \times 10^{-15}$ erg s^{-1}cm^2) from its discovery to date, the X-ray quiescent emission appears to be dominated by a very small spot at $kT \sim 0.3$ keV and of radius ~ 0.16 km (Rea et al. 2013). By modeling the magneto-thermal secular evolution, we infer a realistic age of this souce is inferred to be ~ 550 kyr, and a dipolar magnetic field at birth of 3×10^{14} G (Vigona et al. 2013).

Summary

By considering general relativity effect, we calculated the dipolar toroidal magnetic field decay rates, and investigated the $L_X - L_{rot}$relation of 22 magnetars with soft X-ray luminosities. It is found that, for magnetars with $L_X < L_{rot}$, their observed soft X-ray emissions may come from the rotational energy loss rate, or from magnetosphere flow, and/or from particle wind heating, while for magnetars with $L_X > L_{rot}$, the Ohmic decay of crustal toroidal magnetic fields can provide their observed isotropic soft X-ray luminosities and maintain high thermal temperatures.

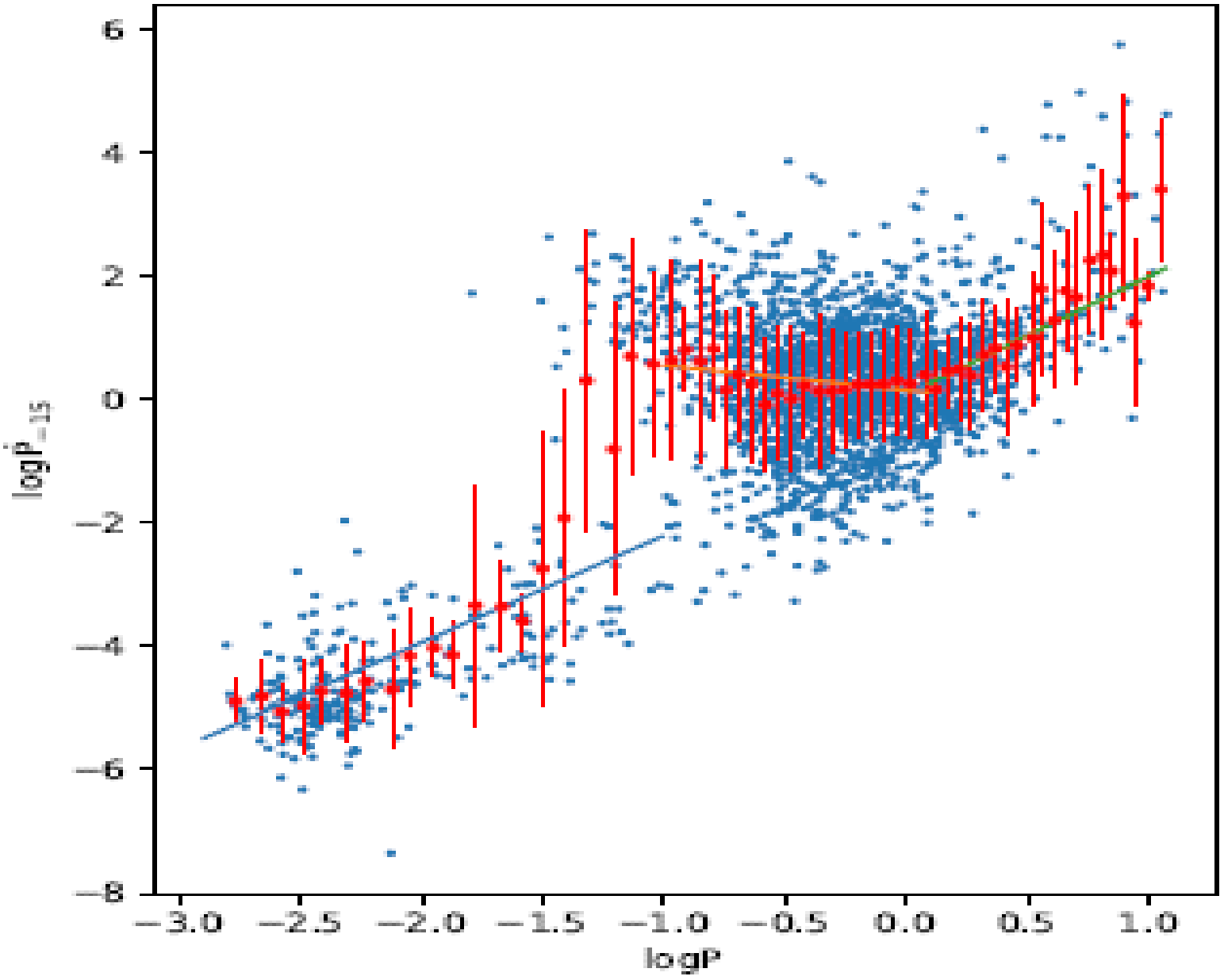
6
4
2
0
−2
−4
−6
−8
−3.0
−2.5
−2.0
−1.5
−1.0
−0.5
0.0
0.5
1.0
logP
$\log \dot{P}_{-15}$